

# I Beg to Diffract: RF Field Programming With Edges

Anurag Pallaprolu, Winston Hurst, Sophia Paul and Yasamin Mostofi

{apallaprolu, winstonhurst, s\_paul}@ucsb.edu, ymostofi@ece.ucsb.edu

University of California Santa Barbara

Santa Barbara, USA

## ABSTRACT

In this paper, we propose a new paradigm in intelligent surface design for field programming and multi-point focusing. We approach this problem from an entirely different vantage point by leveraging edges and the corresponding Geometrical Theory of Diffraction (GTD), allowing us to avoid the use of highly specialized and expensive element designs. More specifically, we show that a lattice of edge elements (*i.e.*, cheap, thin, rectangular metal plates with length long enough as compared to width) can provide a rich repertoire for programming the RF field. When a wave is incident on an edge, a cone of outgoing rays emerges, known as a Keller cone. When considering a lattice of such edge elements, we then have a rich set of “knobs” for RF field programming, via changing the orientation of the edge elements and exploiting the exiting Keller cones. We then show how to electromagnetically model and design a practical edge element. We further propose an efficient algorithm to configure the orientations of the edges to achieve the desired multi-point focusing. We build sample prototypes of our proposed paradigm, using off-the-shelf material (*i.e.*, 7 cent metal plates). We then show several real-world experiments in three different indoor areas, where an edge lattice focuses the transmitted wave of a WiFi card of a laptop on up to and including 4 focal points (maximum achieved in the literature albeit with much more expensive element designs). Overall, the paper shows the rich potential of edges for RF field programming.

## CCS CONCEPTS

• **Hardware** → **Beamforming; Analysis and design of emerging devices and systems; Wireless devices**; • **Networks** → *Physical links*; • **Computer systems organization** → Sensor networks.

## KEYWORDS

Intelligent Electromagnetic Surfaces, Metasurfaces, Keller Cones, Diffraction, Edge Lattice, Edge Element, Beamforming

## ACM Reference Format:

Anurag Pallaprolu, Winston Hurst, Sophia Paul and Yasamin Mostofi. 2023. I Beg to Diffract: RF Field Programming With Edges. In *The 29th Annual International Conference on Mobile Computing and Networking (ACM MobiCom '23)*, October 2–6, 2023, Madrid, Spain. ACM, New York, NY, USA, 15 pages. <https://doi.org/10.1145/3570361.3613266>

## 1 INTRODUCTION

The subject of intelligent electromagnetic surfaces (also known by other names such as Large Intelligent Surfaces (LIS), Intelligent Reflecting Surfaces (IRS), Metasurfaces, Reconfigurable Intelligent Surfaces (RIS), *etc.*) has seen a drastic growth in research activity over the past few years, particularly due to the emergence of the 6G standard [17, 55] and the rapid deployment of 5G communication systems [19, 20, 50]. With the arrival of Massive MIMO [6, 37, 43, 57] as a robust spatial multiplexing backbone for 5G systems, intelligent surfaces are considered to be the next stage of evolution in RF field programming [8, 27] using compact, low-power antenna arrays with re-radiation characteristics.

At its core, an IRS is a two-dimensional array of unit elements with sub-wavelength dimensions, envisioned to smartly control, manipulate, and program the incident electromagnetic field in any desired manner [1, 20, 24, 25, 65]. Intelligent surfaces are thus anticipated to be an integral part of communication systems to assist with scenarios such as creating smart radio environments, high-frequency band communication, localization, and security/privacy, among many other possibilities [9].

We next provide a brief overview of the state of the art, referring the readers to Section 2, which provides a very comprehensive review of the related work. In recent years, there has been a considerable interest in intelligent surfaces and smart radio environments. However, most of such existing work focuses on highly theoretical modeling and simulation-based validation in idealistic settings [7, 14, 18, 45, 48, 70]. When considering work that has successfully demonstrated the potentials of intelligent surfaces via design and implementation, the task of re-steering incident radiation to a *single* direction has been well studied [2, 21, 52, 54], and

---


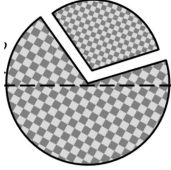
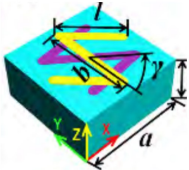
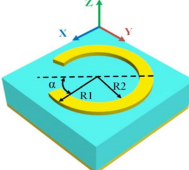
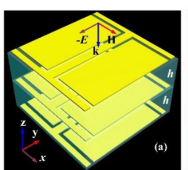
Permission to make digital or hard copies of part or all of this work for personal or classroom use is granted without fee provided that copies are not made or distributed for profit or commercial advantage and that copies bear this notice and the full citation on the first page. Copyrights for third-party components of this work must be honored. For all other uses, contact the owner/author(s).

*ACM MobiCom '23, October 2–6, 2023, Madrid, Spain*

© 2023 Copyright held by the owner/author(s).

ACM ISBN 978-1-4503-9990-6/23/10.

<https://doi.org/10.1145/3570361.3613266>

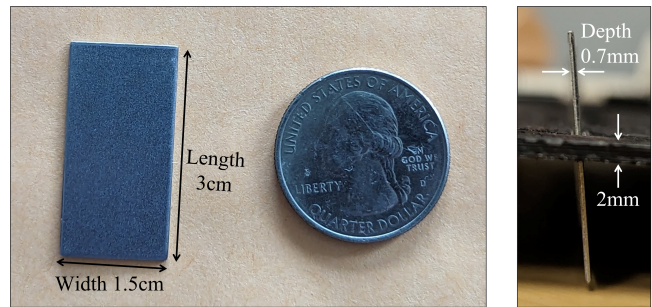
Reference	This Paper	[31]	[62]	[3]	[68]
Frequency	5 GHz	20 GHz	11-13 GHz	13&16 GHz	9-10 GHz
Num. of Elements	484	21,464	3,500	1,600	625
Experimental Environment	Real-world environments	Anechoic chamber	Anechoic chamber	Anechoic chamber	Anechoic chamber
Element Design and Complexity	Bare metal plate costing 7 cents 	Holography-based V-shaped cuts in circular patches 	Z-shaped metal patch on F4B substrate with copper grounding 	C-shaped particle with variable orientation and opening angles 	Transmissive triple-layer meta-atom with multiple resonant modes 
Off-the-shelf element	✓	✗	✗	✗	✗

**Figure 1: Sample of state of the art implementations for multi-point focusing with intelligent surfaces. To the best of our knowledge, table includes all implementations that can achieve four-point/beam focusing.**

commercial prototypes have already begun testing and deployment [46, 47]. Splitting the incident beam into two directions [13], as well as simultaneous transmission and reflection [41, 71], has also been demonstrated in recent work.

While controlling and programming the RF field in any desired manner is one of the envisioned goals of an intelligent surface, re-radiating the incoming wave to multiple directions, *i.e.*, simultaneously focusing at multiple points in space, remains a considerably challenging problem. More specifically, only a small subset of prior work has successfully demonstrated intelligent surface designs capable of focusing at more than one point (see Fig. 1). Furthermore, most work on multi-point focusing has shown focusing at a maximum of two directions [13, 22, 59], while there are only a very small number of works ([3, 31, 62, 68] from the antenna and propagation community) that have shown focusing at the maximum of four directions/locations. However, these works utilize complex and costly unit element design, relying on specialized RF components to achieve focusing at the maximum of four beams. They further deploy a large number of elements and mainly test in highly favorable environments (*e.g.*, anechoic chambers), as opposed to real multipath environments. See Fig. 1, Section 2 and Table 1 for a comprehensive summary of past work.

**Introducing our edge element:** Consider a small, thin metallic plate, as shown in Fig. 2, whose length is large enough as compared to its width such that the diffraction off of its edges becomes the main propagation phenomenon (more on the design specification of such an edge element in Section 3). Such an edge element costs 7 cents, and a lattice of these can be easily put together with off-the-shelf material.

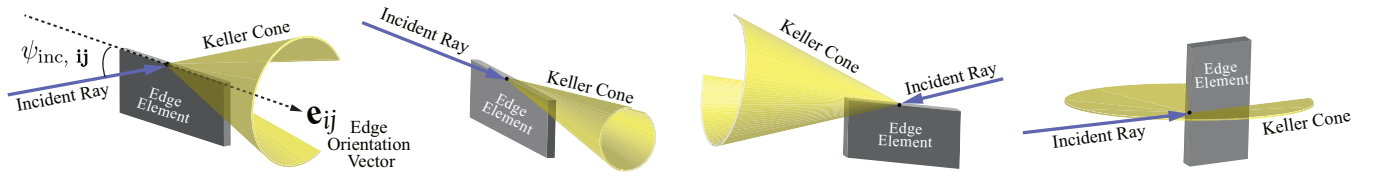


**Figure 2: (left) Size of our practical edge element. (right) Element inserted in 2 mm thick ABS plastic frame.**

In this paper, we pose the following question: **what can a number of such edge elements do for RF field programming?** Can they, for instance, passively focus the transmitted signal towards multiple focal points simultaneously?

We then set forth a new idea for near-field multi-point focusing which radically departs from traditional intelligent surface design approaches. More specifically, we show that a 2D lattice of edge elements has great potential for programming the RF field and generating multiple simultaneous focal points, which can be beneficial for tasks such as low-power spatial-modulation in 5G/6G systems, enhanced EM jamming and drone swarm navigation, among other use cases. This is due to the fact that an edge interacts differently with the incoming wave than the typical surface elements. More formally, we have the following:

**Keller Cones:** Consider a wave incident on an edge point (*i.e.*, a point of discontinuity in the surface normal's direction). A cone of outgoing rays emerges according to Keller's Geometrical Theory of Diffraction (GTD) [34, 36]. The angle



**Figure 3: Interaction of an incident ray with an edge leads to a cone of outgoing rays, known as the Keller cone. The axis of the cone is the edge, and the angle of the cone is the angle of incidence. See color PDF for proper viewing.**

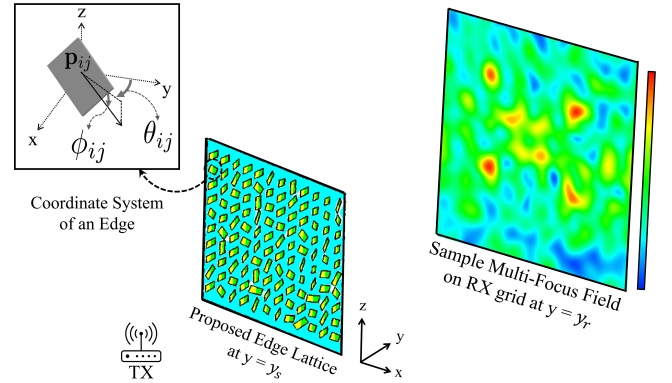
of the cone is equal to the angle between the incident ray and the edge (which is also the axis of the cone). Fig. 3 shows sample interactions of an incoming wave with an edge and the resulting Keller cones.

As the edge orientation changes, the exiting Keller cone guides the energy in different directions, allowing for rich programmability of the electromagnetic field. When considering a lattice of edge elements, we then have a set of “knobs” for controlling the RF field. In other words, by changing the orientation of the edge elements in the lattice, one can generate new RF fields. Fig 4 shows a high-level schematic of our proposed paradigm where a lattice of edges in front of an RF source focuses the transmitted signal towards multiple focal points simultaneously.

We next discuss our main contributions in detail:

#### Statement of Contributions:

- We propose a new paradigm in intelligent surface design for field programming and multi-point focusing that leverages edges and the corresponding Geometrical Theory of Diffraction (GTD). More specifically, we show that a lattice of edge elements (*i.e.*, thin rectangular plates with length long enough as compared to width) can provide a rich repertoire for programming the RF field, via changing the orientation of the edge elements and exploiting the exiting Keller cones.
- We leverage the GTD to electromagnetically model and design a practical edge element, which is fully passive.
- We propose an efficient algorithm to configure the orientations of the edge elements of the lattice such that the diffracted fields off of the whole lattice constructively interfere at a set of desired focal points. In doing so, we further propose an efficient Metropolis-filter-based approach, inspired by log-linear learning [58], to partition the edge elements among the focal points.
- We extensively validate the proposed paradigm with several experiments (13 total) in 3 different indoor environments. Specifically, we build sample prototypes of our proposed design, using off-the-shelf material. Each edge element is a 3 cm × 1.5 cm steel plate costing 7 cents to make and is held in place with a 2 mm thick ABS plastic frame (see Fig. 2). We then show several experiments where square lattices of size 20 × 20, 22 × 22, or 12 × 12 focus the transmitted wave of a WiFi card of a laptop on



**Figure 4: High-level schematic of our proposed paradigm – A lattice of edge elements is placed in front of a transmitter in order to focus the transmitted signal into multiple focal points. The edge orientations are then configured to achieve the given multi-focusing task. See color PDF for proper viewing.**

up to and including 4 focal points, with a peak gain of 10.9 dB in the CSI magnitude.

- We further experimentally show the impact of many different factors, such as size of the lattice, steering angle of the focal point, and environmental factors, on the performance of the proposed approach. All our measurements are carried out using commodity transceivers and take place in indoor spaces, *i.e.*, in areas that naturally exhibit significant multipath activity. Furthermore, no prior knowledge of the experimentation environment is needed to configure the lattice.
- To the best of our knowledge, no prior work has achieved simultaneous focusing at four points without the use of highly specialized element designs. Overall, the paper shows the rich potential of edges for field programming and can open up new possibilities in the area of intelligent surfaces. It is worth noting that we do not propose abandoning traditional non-edge surfaces but rather set forth a new possibility that can contribute to and advance the area of intelligent surfaces.

## 2 RELATED WORK

The architecture of an intelligent electromagnetic surface takes its roots in the domains of active array, reflectarray, and array lens design [29, 61]. Active arrays, also known as Elec-

Ref.	# Elements	# Beams	# Elements/Beam	Max Steer. Angle	Resolution	Frequency	# Experiments
<b>Our Paper</b>	484	4	<b>121</b>	<b>53°</b>	<b>0.06 rad</b>	<b>5.18 GHz</b>	<b>13</b>
[31]	21,464	4	5,366	28°	0.12 rad	20 GHz	1
[62]	3,500	4	875	45°	0.13 rad	11-13 GHz	1
[3]	1,600	4	400	39°	0.07 rad	13 & 16 GHz	2
[68]	625	4	156.25	30°	0.13 rad	9.6 GHz	2
[60]	512	2	256	45°	0.07 rad	5.8 GHz	2
[69]	408	1	408	55°	0.12 rad	4.8 GHz	4
[64]	2,400	1	2,400	32°	0.09 rad	672 GHz	5
[40]	48,400	1	48,400	72°	0.09 rad	1 THz	4

**Table 1: Comparison of performance metrics with state of the art. When explicitly not stated, we use experimental results of prior work to estimate metrics. We note all our experiments are performed in multipath-rich areas. See Fig. 1 for comparison of design complexity and experiment area with past work that achieve 4 beams.**

tronically Steerable Arrays (ESA), allow for both amplitude and phase control of the radiating elements for the task of generating a customized field. However, these arrays are very expensive, require a complex, elaborate beamforming network (BFN) [10], and were thus originally intended for military and satellite communication purposes. In a bid to eliminate the complexity of BFN design, reflectarrays [4, 30, 51] and array lenses [15, 16, 44] utilized a dedicated feed as the primary RF power source for a spatially separated antenna array, and the obvious next step involved directly controlling the re-radiated field of the array itself. For instance, [33] is an interesting early attempt at a smart reflector design composed of phase shifting units on a conformal surface to redirect an incident signal in a specified direction. Other early work on smart surfaces include [38, 63], which proposed using a large number of commodity antenna units, colocated with low-resolution phase shifters, as spatially extended programmable relays.

Since 2017, there has been a considerable interest in intelligent surfaces and smart radio environments from a number of communities. In the communication community, much of the work on this topic mainly focuses on highly theoretical modeling, and simulation-based validation in idealistic settings [7, 14, 18, 45, 48, 70]. For instance, they primarily focus on establishing performance metrics in a context that is agnostic to the actual design of a practical surface.

On the other hand, ease of access to PCB fabrication technology has enabled some recent work to design and implement intelligent surfaces. In particular, there has been considerable work on steering the incident energy towards a *single* direction by constructing and deploying designs using patch antenna arrays. For instance, [54] used a  $10 \times 10$  array of inset-fed patch antennas with 7 available phase offsets to strategically reflect a horn antenna's incident energy in one direction. Along the same line, [21] implemented three  $4 \times 4$  "tiles" of patch antennas each equipped with 4 available phase

shifts to improve a single link's SNR by 5.5 dB. Other work, such as [2] demonstrated single point focusing by utilizing a very large matrix of 3,200 ON/OFF modulated elements to boost signal strength. [52] is another interesting example of a reflectarray that exploits the delay of the RF path off of a metallic surface overlaid with a variable-depth dielectric to improve the quality of one link. Some of the earlier work further focused on generating a very coarse-grained spatial RF field with customized static 3D reflectors [11, 35, 67], while recent efforts aim to achieve more precise tasks such as splitting of an incident beam into two directions [13] or simultaneous transmission and reflection [41].

In this paper, we are interested in programming the RF field such that multi-point focusing on any set of desired locations can be achieved. Simultaneous focusing at multiple points in space, however, remains a considerably challenging problem, and to the best of our knowledge, only a small subset of prior work has successfully demonstrated intelligent surface designs capable of this task (see Fig. 1). Most work on multi-point focusing has shown simultaneous focusing on the maximum of two directions (examples include [13, 22, 59]), while there are only a handful of works ([3, 31, 62, 68] from the antenna and propagation community) that have shown focusing at the maximum of four directions/locations. However, as summarized in Fig. 1, to achieve 4-point focusing, these works utilize very complex and costly element design, relying on exotic antenna designs and specialized RF components for their element, as opposed to using off-the-shelf material.

For instance, [3] utilizes a C-shaped ring particle as an antenna element whose amplitude and phase response is modulated by controlling the extent of opening in the ring, which requires high precision PCB manufacturing tolerance that can drive up the cost. [31, 62] on the other hand require precise angular placement of Z-shaped/V-shaped antenna elements on a substrate which would add further complexity

to manufacturing. [68] considers a multi-layer resonant cavity as the re-radiating element, which is sensitive to vertical alignment and demands high quality fabrication techniques to achieve accurate layering.

Most aforementioned work that achieved 4 focus directions/points also utilize a large number of elements, *e.g.*, 21,464 in [31], 3,500 in [62], and 1,600 in [3]. Furthermore, they only test in highly favorable environments (*e.g.*, anechoic chambers), as opposed to real-world environments that can suffer from multipath, while also utilizing specialized transmit antennas, as opposed to off-the-shelf devices.

In this paper, we ask “what can a number of edge elements do for field programming?” Can they, for instance, focus the signal radiated from an off-the-shelf transmitter, such as the WiFi card of a laptop onto any given set of points? We then show that a 2D lattice of cheap \$0.07 off-the-shelf edge elements can successfully achieve multi-point focusing, fully passively and in harsh indoor environments.

While each element of a typical intelligent surface has an omni-directional pattern, our proposed edge lattice concept steps away from the traditional element design paradigm to instead consider thin rectangular prisms with a length large enough, as compared to the width, such that diffraction off of the edges is the main propagation phenomenon.

Such an edge element then diffracts the incoming wave according to the GTD and the associated Keller cones, resulting in directional radiation footprints that are localized in space (See Fig. 3 for examples). As the edge element’s orientation changes, the exiting Keller cone guides the energy in different directions, allowing for rich programmability.

In stark contrast to existing approaches, our proposed paradigm requires relatively few and remarkably simple elements to achieve the difficult task of simultaneous multi-point focusing, easily achieving the best possible in the literature (4-point focusing) with off-the-shelf elements. Furthermore, we demonstrate our architecture’s focusing capability in relatively unfavorable environments, *i.e.*, using commodity WiFi transceivers and in the presence of considerable multipath interference.

While Fig. 1 discussed prior work on four-point focusing from the angle of design complexity, Table 1 further provides a detailed metric-wise comparison. In summary, we achieve

**Best median resolution (0.06 radians)**, while operating at a much lower frequency and with many fewer elements.

**Maximum steering angle of 53°**. While [40] shows a larger angle, it only shows single-point focusing with a very large number of elements.

**13 experiments in multipath-rich indoor settings**, using a COTS WiFi antenna as the transmitter (see Sec. 5.3). Other work use highly directional horn antenna feeds, and experiment either in simulation or in environments with minimal multipath (*e.g.*, anechoic chambers).

**Fewest number of elements per beam of 121**. We note that [66] (published after writing of this paper) has shown 9 beams with 1,369 elements (156.25 elements per beam) in anechoic chambers, but with minimal validation in real world environments. It further uses complex 4-layer double-square-ring antennas.

Overall, our work constitutes a notable contribution to this field not only due to the novel paradigm and low cost design, but also in terms of the achieved robust performance.

We next start by modeling and designing our edge lattice.

### 3 EDGE LATTICE MODELING & DESIGN

Consider a system consisting of a single isotropic source (TX) and a number of edge elements arranged in a two-dimensional lattice, as shown in Fig. 4. The source is located at a point  $\mathbf{x}_{\text{src}} \in \mathbb{R}^3$ , and the edge element in row  $i$  and column  $j$  of the lattice is located at  $\mathbf{p}_{ij} \in \mathbb{R}^3$ . Let  $\theta_{ij}$  and  $\phi_{ij}$  denote the azimuth and elevation angles of the edge element at  $\mathbf{p}_{ij}$ , as indicated in the figure. Consider a given RF field, consisting of multiple focal points that we are interested in generating. In this paper, we then want to find the edge lattice configuration (*i.e.*, angles of all the edge elements) that will result in the desired RF field. Since we are laying out a new concept, that a 2D lattice of edge elements can generate diverse RF fields, we show the details of our proposed paradigm when generating a field across a 2D plane. However, we emphasize that the methodology can be extended to 3D. For the ease of developing our mathematical foundation, we consider a 2D plane parallel to the edge lattice, where we are interested in generating a desired multi-focus field. However, as we see in our experiments, the 2D plane can be in other locations/orientations with respect to the edge lattice.

#### 3.1 Modeling of a Single Edge Element

Consider a 2D plane at  $y = y_r$ , where we are interested in generating a desired multi-focus field, as shown in Fig. 4. We refer to this plane as the RX grid. In this paper, we consider the 2D plane to be on the opposite side of the transmitter, without loss of generality. According to Born approximation [12], the total complex baseband signal at any point on the receiver grid can be written as the linear sum of the direct path from the transmitter and the paths diffracted from each of the edge elements. We next formally model the interaction of the transmitted electromagnetic waves with each edge element.

The complex baseband signal of an RF wave of wavelength  $\lambda$  originating from an isotropic TX at  $\mathbf{x}_{\text{src}}$  and incident on an edge element at  $\mathbf{p}_{ij}$  is given by,

$$F_{\text{src}}(\mathbf{p}_{ij}, \mathbf{x}_{\text{src}}) = \frac{\sqrt{P_{\text{src}}}}{\sqrt{4\pi\|\mathbf{x}_{\text{src}} - \mathbf{p}_{ij}\|}} e^{-j2\pi\|\mathbf{x}_{\text{src}} - \mathbf{p}_{ij}\|/\lambda} \quad (1)$$

where  $P_{\text{src}}$  is the transmit power. We model the interaction of the edge element with this incoming incident wave using the

Geometrical Theory of Diffraction (GTD) [34, 36]. As shown in Fig. 3, GTD models the scattered field off of an edge as a cone of outgoing rays known as the Keller cone. Let vector  $\mathbf{e}_{ij}$  denote the axis of the cone, which describes the physical orientation of the edge. Then the angle of the cone is equal to the angle of incidence,  $\psi_{inc,ij}$ , as illustrated in Fig. 3 (left). Importantly, both  $\mathbf{e}_{ij}$  and  $\psi_{inc,ij}$  are determined by  $\theta_{ij}$  and  $\phi_{ij}$ , with  $\mathbf{e}_{ij} = [\cos\phi_{ij}\sin\theta_{ij}, \cos\phi_{ij}\cos\theta_{ij}, \sin\phi_{ij}]$  and:

$$\psi_{inc,ij} = \arccos \left\{ \frac{\langle \mathbf{p}_{ij} - \mathbf{x}_{src}, \mathbf{e}_{ij} \rangle}{\|\mathbf{p}_{ij} - \mathbf{x}_{src}\| \|\mathbf{e}_{ij}\|} \right\}$$

where  $\langle \cdot, \cdot \rangle$  represents the inner product. Consequently, by controlling the orientation of the edge element, we control the direction and spread of the exiting Keller cone.

To check if a given receiver point on the RX grid lies on the cone, we compare  $\psi_{inc,ij}$  to the angle between the edge element orientation vector,  $\mathbf{e}_{ij}$ , and the vector from the edge element location  $\mathbf{p}_{ij}$  to the receiver location  $\mathbf{x}$ . If equal, the receiver point is said to lie on the corresponding cone. This can be stated formally as

$$I(\mathbf{x}, \mathbf{p}_{ij}, \mathbf{e}_{ij}) = \begin{cases} 1 & \text{If } \arccos \left\{ \frac{\langle \mathbf{x} - \mathbf{p}_{ij}, \mathbf{e}_{ij} \rangle}{\|\mathbf{x} - \mathbf{p}_{ij}\| \|\mathbf{e}_{ij}\|} \right\} = \psi_{inc,ij} \\ 0 & \text{Otherwise} \end{cases} \quad (2)$$

Thus, the complex electric field at a general receiver location  $\mathbf{x}$ , due to the Keller cone off of an edge element located at  $\mathbf{p}_{ij}$ , with an edge element orientation  $\mathbf{e}_{ij}$ , is given by:

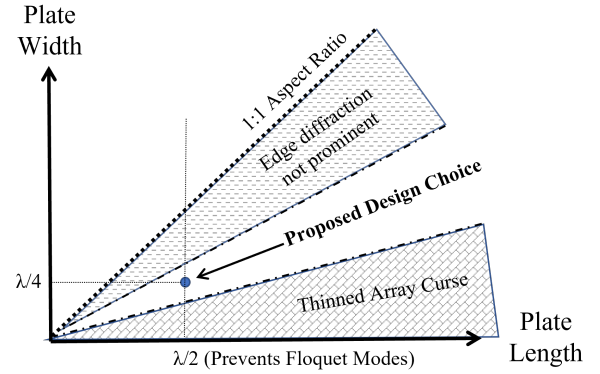
$$F_{cone}(\mathbf{x}, \mathbf{p}_{ij}, \mathbf{e}_{ij}) = F_{src}(\mathbf{p}_{ij}, \mathbf{x}_{src}) \frac{D e^{-j2\pi\|\mathbf{x} - \mathbf{p}_{ij}\|/\lambda}}{\sqrt{\|\mathbf{x} - \mathbf{p}_{ij}\|}} I(\mathbf{x}, \mathbf{p}_{ij}, \mathbf{e}_{ij}), \quad (3)$$

where  $D$  is the Sommerfeld diffraction coefficient [34]. The Keller cone model discussed in [34] is presented for an infinitesimal edge, such that each point along the edge produces its own cone. However, as the edge elements of our lattice are quite small, we treat the diffraction pattern from each edge element as a single cone.

### 3.2 Design of an Edge Element

In this section, we discuss the practical design aspects of our edge element and present a set of parameters suitable for it. We consider each edge element as a thin rectangular metallic plate, as shown in Fig. 2.

The most critical design parameter is the ratio of the length of the edge element to its width, which determines how close to an ideal edge the element will be. The aspect ratio of the edge element should be large, *i.e.*, the length should be much longer than the width, to ensure that diffraction off of the edge is the dominant mode of electromagnetic interaction. However, for a given width, as the length becomes longer, each edge element needs more space around it so that it can rotate to any given angle. This results in a greater percentage of incident energy simply passing through our edge lattice rather than being intercepted by it. In the context of antenna



**Figure 5: Design space for the sizing of the edge element. If the plate is too wide, there is no prominent edge. If the plate is long but too thin, there is less energy intercepted by the edge lattice.**

array theory, this is similar to what is known as the *thinned-array curse* [23], and the energy that is not intercepted by the elements manifests itself as sidelobe levels in the scattering. As such, our design choice should strike a balance between these two factors. In practice, we find that an aspect ratio of 2:1, *i.e.*, a length twice as long as the width, works well.

There are many length-width pairs that satisfy the 2:1 aspect ratio. As discussed above, the length of the edge element determines the inter-element spacing on the lattice, and for an array operating at wavelength  $\lambda$ , it is well known that a  $\lambda/2$  spacing between elements avoids Floquet diffraction lobes as it satisfies the spatial Nyquist sampling rate [39, 54]. Furthermore, empirical results from the literature corroborate that elements of this length result in strong interaction with the electromagnetic field [2]. Consequently, we set the length of each edge element to  $\lambda/2$  and, in order to realize the 2:1 aspect ratio, the width to  $\lambda/4$ . At our operating frequency of 5 GHz, this corresponds to a 3 cm  $\times$  1.5 cm edge element. We note that since the width is  $\lambda/4$ , the element appears as a single edge to the incoming wave. Fig. 5 summarizes the design space and the corresponding trade-offs.

Finally, for completeness, we note that edge diffraction can be well modeled using GTD, not only at this scale [28], but at other frequencies [53, 56]. Diffraction has also been used in other domains, *e.g.*, in a completely different context/setup of tracing of edges of everyday objects [49].

## 4 RF FIELD PROGRAMMING USING A LATTICE OF EDGES

In this section, we lay the foundation of generating a multi-focus field with a lattice of edge elements. More specifically, we propose an algorithm that determines the three-dimensional orientations (*i.e.*, azimuth and elevation angles) of the edge elements of a 2D lattice so they can create a desired multi-focus field.

Without loss of generality, we assume that the transmitter (TX) is located at the origin of the coordinate system. The lattice  $\mathcal{M}$  of  $N \times N$  edge elements is then positioned in the X-Z plane at  $y = y_s$ , with the goal of steering the energy radiated by the TX such that a desired multi-focus pattern is achieved at a 2D plane  $RX$ , as shown in Fig. 4. Without loss of generality, we present the mathematical details of this section assuming that  $RX$  is at  $y = y_r > y_s$ . However, as we shall see in our experiments, the receiver plane need not be parallel to the edge lattice. We index each edge element in our lattice by  $(i, j)$ , for  $1 \leq i, j \leq N$ .

The problem of finding optimum edge element orientations to achieve any given multi-focus field is considerably challenging. While one can pose it as a general optimization problem and attempt to solve it using heuristic approaches, such a strategy may not converge to an acceptable solution. Furthermore, the computational complexity of solving such a general optimization problem can be prohibitive. In this section, we thus show how we can efficiently solve this multi-focus optimization problem by dissecting it into two parts of 1) focusing on a single point and 2) edge lattice partitioning among multiple focal points.

#### 4.1 Single Point Focusing

Let  $\mathbf{f} \in RX$  denote the focal point of interest. We first devise an efficient strategy to steer the Keller cone off of a single edge element to  $\mathbf{f}$ . We then use this strategy to show how we can effectively select the orientations of the edge elements in the entire lattice to achieve this focusing.

**4.1.1 Steering a Cone to a Point.** To achieve focusing, we must first be able to orient an edge element such that the Keller cone off of its edge impinges on the target point. The following theorem demonstrates how this can be achieved in an efficient manner.

**THEOREM 4.1.** *Consider an edge element located at  $\mathbf{p}_{ij}$  with an edge vector of  $\mathbf{e}_{ij}$  (see Fig. 3 (left) for illustration). The resulting Keller cone off of this edge element passes through location  $\mathbf{f}$  if the following holds:*

$$\mathbf{e}_{ij} = \frac{\mathbf{f} - \mathbf{p}_{ij}}{|\mathbf{f} - \mathbf{p}_{ij}|} + \frac{\mathbf{p}_{ij}}{|\mathbf{p}_{ij}|}.$$

**PROOF.** From Keller's Law of Edge Diffraction [34], we know that the angle of the Keller cone is equal to the angle of incidence. If the Keller cone must pass through  $\mathbf{f}$ , we have:

$$\begin{aligned} \left\langle \frac{\mathbf{p}_{ij}}{|\mathbf{p}_{ij}|}, \mathbf{e}_{ij} \right\rangle &= \left\langle \frac{\mathbf{f} - \mathbf{p}_{ij}}{|\mathbf{f} - \mathbf{p}_{ij}|}, \mathbf{e}_{ij} \right\rangle \\ \implies \left\langle \frac{\mathbf{p}_{ij}}{|\mathbf{p}_{ij}|} - \frac{\mathbf{f} - \mathbf{p}_{ij}}{|\mathbf{f} - \mathbf{p}_{ij}|}, \mathbf{e}_{ij} \right\rangle &= 0 \end{aligned}$$

From the parallelogram law of vector addition, a vector normal to the difference of two unit vectors is given by their sum, and this completes the proof.  $\square$

While this theorem gives an orientation for each edge such that its Keller cone passes through a given point in space, steering the cones of all the edge elements to a target point will clearly not work, as the paths on different cones may destructively interfere with each other. We next discuss how to optimize the group behavior of the edge elements for proper focusing.

---

#### Algorithm 1: Single Point Focusing with a Lattice of Edges

---

```

1: for edge element  $(i, j) \in \mathcal{M}$  at location  $\mathbf{p}_{ij}$  do
2:   Using Theorem 4.1, find an orientation such that
   edge element's Keller cone impinges on the target.
3:   if resulting complex-valued edge diffraction path has
   positive projection on direct path from TX then
4:     Orient edge element's cone to impinge on target,
     i.e., set  $\mathbf{e}_{ij} = \frac{\mathbf{f} - \mathbf{p}_{ij}}{|\mathbf{f} - \mathbf{p}_{ij}|} + \frac{\mathbf{p}_{ij}}{|\mathbf{p}_{ij}|}$ .
5:   else
6:     Put element in idle state, i.e.,  $\mathbf{e}_{ij} = [0, 0, 1]$ .
7:   end if
8: end for

```

---

**4.1.2 Selecting Edge Elements for Focusing.** Once we have determined the orientation of each edge element that will result in the corresponding Keller cone passing through the target point  $\mathbf{f}$ , we need to decide which of the elements to select for focusing at  $\mathbf{f}$ . To do so, we select only those edge elements that positively reinforce the direct path from the TX to  $\mathbf{f}$ . More specifically, we check if the complex field of the path on the Keller cone from an edge element,  $F_{\text{cone}}(\mathbf{f}, \mathbf{p}_{ij}, \mathbf{e}_{ij})$ , has a positive projection onto the direct path field  $F_{\text{src}}(\mathbf{f}, \mathbf{x}_{\text{src}})$  in the absence of the edge lattice, i.e., purely due to the transmitter. Mathematically, this can be written as:

$$\Re\{F_{\text{cone}}^*(\mathbf{f}, \mathbf{p}_{ij}, \mathbf{e}_{ij})F_{\text{src}}(\mathbf{f}, \mathbf{x}_{\text{src}})\} > 0 \quad (4)$$

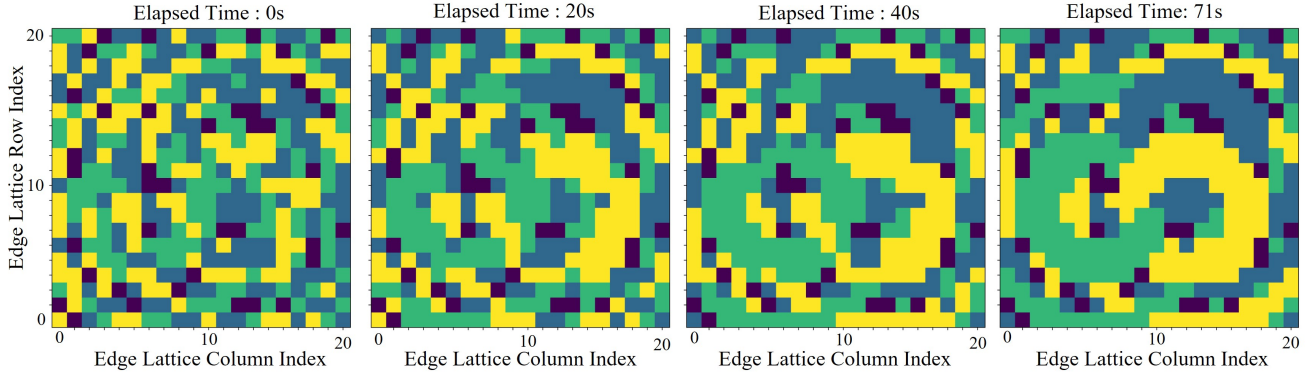
where  $\Re\{\cdot\}$  denotes the real part of the argument and  $*$  denotes complex conjugation. It is worth noting that approaches along the lines of reinforcing the direct path have been used in the literature [2, 38, 63].

**Idle Edge Elements:** For the edge element locations that do not satisfy the aforementioned criterion, we need to set them in an "idle" state. We have found empirically that setting these elements vertically upwards such that  $\mathbf{e}_{ij} = [0, 0, 1]$ , amplifies the focusing of our lattice. The rightmost scenario in Fig. 3 shows this orientation and its corresponding cone. We thus use such an edge state as our idle state.

Algorithm 1 summarizes our proposed method for single point focusing using edge elements.

#### 4.2 Multi-Point Focusing

Next, let us consider the general problem of focusing on  $K$  given points of interest,  $\mathbf{f}_i \in RX$ ,  $1 \leq i \leq K$ , using a lattice of edge elements. We next show how to efficiently decide on



**Figure 6: Sample demonstration of the convergence of Algorithm 2 to partition a  $20 \times 20$  edge lattice for simultaneous focusing at 3 target points. The plots show the 2D edge lattice such that cells of the same color, for yellow, green and navy, indicate edge elements that are assigned to the same target point, while black cells indicate edge elements that are idle for this focusing. As can be seen, Algorithm 2 maximizes the contiguity of each partition while balancing the size of the partitions. See color PDF for proper viewing.**

the orientation of all the edge elements to accomplish this. In doing so, we first show how to partition the edge elements to subsets such that each subset focuses on one of the given focal points (plus an idle subset). Once this is accomplished, we can use the proposed approach of the previous section to set the orientations of the edge elements of each subset so they focus on their corresponding focal point.

---

**Algorithm 2:** Edge Lattice Partition Formation by Metropolis Random Walk

---

- 1: **Input:** Maximum number of iterations,  $C_{iters}$
  - 2: **Output:** Partition assignment matrix  $A = [a_{ij}]$
  - 3: Initialize the assignment matrix  $A$  by sampling uniformly from  $\mathcal{T}_{ij} \forall i, j$ .
  - 4: Initialize iteration count  $c = 1$ .
  - 5: **while**  $c \leq C_{iters}$  **do**
  - 6:   Randomly choose an edge element  $(i, j)$ .
  - 7:   **if**  $|\mathcal{T}_{ij}| > 0$  **then**
  - 8:     For each possible assignment, evaluate the objective in (5), keeping the assignments for all other elements fixed.
  - 9:     Sample  $a_{ij}$  from the corresponding Boltzmann distribution with temperature  $T = 10 \log(c)$ .
  - 10:   **end if**
  - 11:   Increment  $c$ .
  - 12: **end while**
- 

#### 4.2.1 Partitioning Edge Elements Among Multiple Targets.

We first partition our edge elements into mutually exclusive subsets, where one subset corresponds to the edge elements in the idle state, while each of the others corresponds to one of the  $K$  target points. Formally, we have  $\mathcal{M} = \bigcup_{i=0}^K \mu_i$ , where  $\mathcal{M}$  is the set of all edge element indices,  $\mu_i$  for  $i > 0$ , is the partition associated with the  $i^{\text{th}}$  focal point, and  $\mu_0$

are edge elements in the idle state. To ensure fair resource distribution, we consider the scenario in which equal number of edge elements are allocated to each focal point. This can be easily modified in our optimization, if needed. Furthermore, we design our partitions to be spatially contiguous, *i.e.*, the edge elements that are tasked to focus at the same point are spatially grouped.

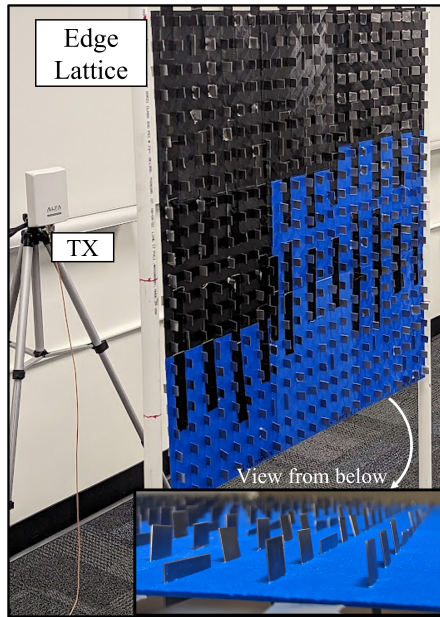
To formalize our optimization problem, we first introduce some relevant notation. Let  $\mathcal{T}_{ij} \subseteq \{1, \dots, K\}$  be the set of targets to which the edge element at  $(i, j)$  can positively contribute according to Equation 4. Furthermore, for  $(i, j) \in \{(i, j) \mid |\mathcal{T}_{ij}| > 0\}$ , let  $a_{ij} \in \mathcal{T}_{ij}$  indicate the target to which edge element  $(i, j)$  is eventually assigned (each edge element is only assigned to a maximum of one target). Our partitioning task can then be formalized as follows:

$$\min_{a_{ij} \in \mathcal{T}_{ij}} \left( \frac{1}{2} \sum_{i,j} v_{ij} + \max_{k,l \in \{1, \dots, K\}} (|\mu_k| - |\mu_l|) \right), \quad (5)$$

where  $v_{ij}$  is the number of neighbors of  $(i, j)$  that belong to a partition different from  $a_{ij}$ . Thus, the first term in the objective encourages partitions that are spatially connected while the second term, which gives the largest pairwise difference in partition sizes, balances the number of assigned edge elements per focal point.

The problem in (5) is a non-convex, combinatorial problem. We next propose an efficient way of solving this problem, which converges very quickly. Inspired by log-linear learning [58], we find approximate solutions using a random walk with a Metropolis filter. Similar to Simulated Annealing, our approach works by defining a Markov chain over the solution space with time-varying transition probabilities. Initially, the walk is almost uniformly random, but over time, greater weight is given to transitions that lead to better values of the





**Figure 7:** A  $22 \times 22$  edge lattice placed in front of a transmitter. The inset shows a close-up of part of the lattice to better highlight different edge orientations. See color PDF for proper viewing. Note that different colors of the ABS plastic are simply due to material availability and are not part of the edge lattice design.

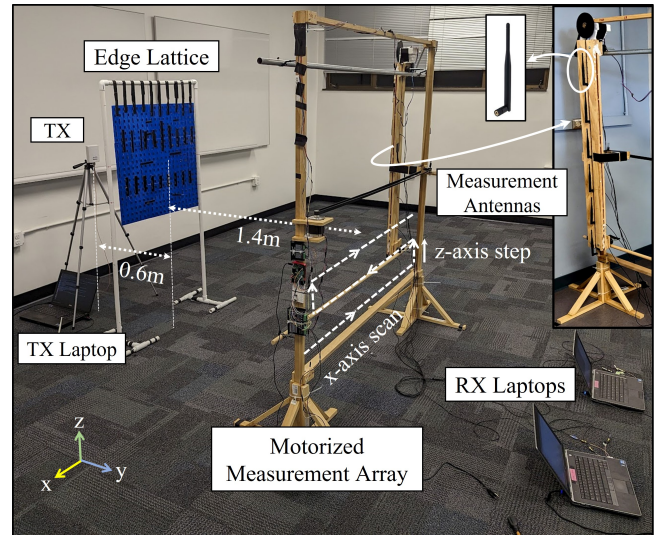
objective function. In the limit, the walk will almost surely converge to an optimal solution. Algorithm 2 summarizes the details. Fig. 6 plots the state of edge lattice partitioning across  $C_{\text{iters}} = 1.8 \times 10^6$  iterations for  $K = 3$  focal points and with  $N = 20$  as the lattice dimension. We see that the algorithm can find partitions that meet our design goals in 71 seconds on a 4<sup>th</sup> generation Intel CPU. In Section 6, we discuss other objective alternatives to Eq. 5.

## 5 EXPERIMENTAL VALIDATION

We next extensively evaluate the performance of our proposed paradigm for multi-point focusing with several real-world experiments. We start by describing our manufacturing pipeline, followed by our experimental setup. We then present several empirical results (*i.e.*, 13 experiments) to demonstrate simultaneous focusing on up to and including four points, with commodity WiFi transceivers, and in indoor areas that exhibit considerable multipath. Our results include testing the proposed approach in 3 different indoor environments as well as showing the performance for wide-angle steering. The impact of several factors, such as lattice size and clutter, is also evaluated. We next start by describing our manufacturing process and experimental setup.

### 5.1 Edge Lattice Manufacturing Pipeline

Our edge elements are constructed by cutting rectangles of dimensions  $3 \text{ cm} \times 1.5 \text{ cm}$  from 0.7 mm thick sheets of

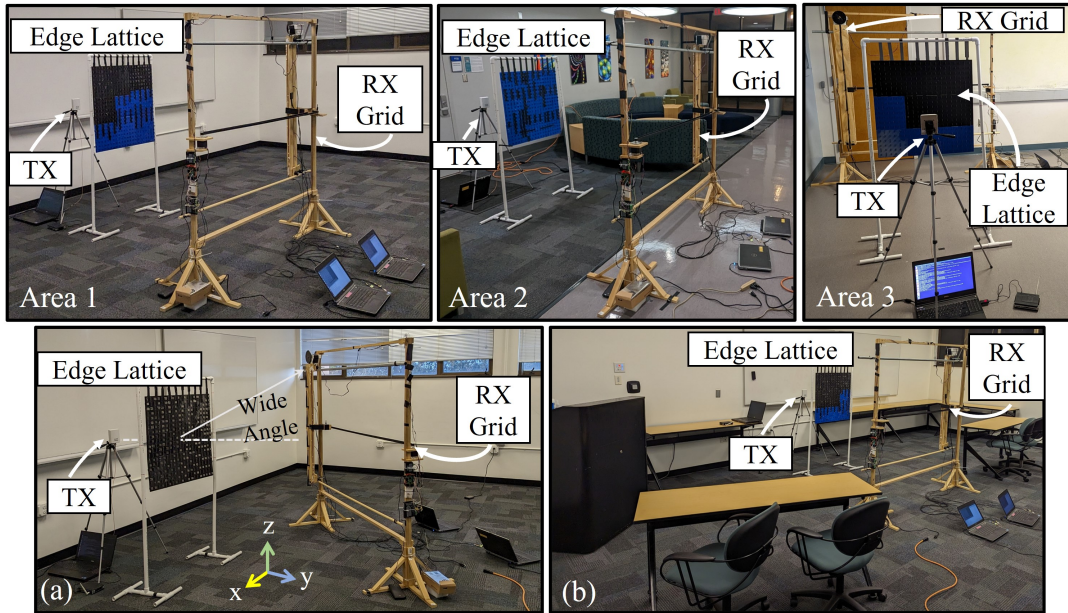


**Figure 8:** Experimental setup in Area 1, consisting of an off-the-shelf TX (WiFi card of a laptop) and the edge lattice. The figure further shows a motorized receiver (RX) array designed to measure the generated field and confirm that the desired multi-point focusing has been achieved. Inset to the top-right shows the side view of the measurement array carriage. See color PDF for proper viewing.

22GA weldable steel (see Fig. 2). As summarized in Fig. 1, in stark contrast to expensive customized element designs of the state of the art approaches for multi-point focusing, each of our edge elements cost \$0.07 to make. For holding the edge elements, we employ a 2 mm thick Acrylonitrile Butadiene Styrene (ABS) plastic frame that has angled slots through it, as shown in Fig. 7. The frame serves the dual purpose of placing the edge elements in the right locations and orienting them in their optimized configurations. We next detail the construction process of this frame. We model an edge lattice in Autodesk Fusion 360, where a Boolean subtraction operation is performed to cut slots into a 2 mm thick solid rectangular frame, with the 3D model of the edge lattice as the cutting tool. The subtracted model is then 3D printed with ABS plastic filament, using a Stratasys F270 3D printer. The entire ABS frame is partitioned into 9 sub-frames for printing, which are then taped together to complete the structure. Finally, the edge elements are inserted into the frame to complete the lattice assembly.

### 5.2 Experimental Setup

As illustrated in Fig. 8, our setup consists of a transmitter (TX) and our proposed edge lattice. To measure the created field, we have built a motorized measurement array of receiver antennas that synthesizes a 2D RX grid. The TX is an off-the-shelf panel antenna (as shown in the figure) and it continuously transmits WiFi packets at the 5.18 GHz band.



**Figure 9: (top) Experimental areas – Conference room (Area 1), lobby (Area 2) and laboratory (Area 3) and (bottom): (a) Wide-angle focusing in Area 1, and (b) Adding additional clutter near the setup of Area 1 to test the impact.**

The antenna is mounted 106 cm above the ground and placed 60 cm behind the edge lattice. To measure the generated field and evaluate the quality of multi-point focusing, we have synthesized an RX measurement array as detailed next.

**Measurement Receiver Array:** The receiver array consists of six omni-directional antennas connected to 2 laptops and stacked vertically with a spacing of 20 cm. The array is mounted on a motorized scaffold, and the RX grid is synthesized by interleaving horizontal scans with vertical steps to scan a new set of parallel rows after every vertical step, as indicated in Fig. 8. The movement is controlled by stepper motors that precisely actuate the array with timing pulleys. With a runtime of 2.5 min. per grid, our motorized apparatus can rapidly sample the field on a  $1.36\text{ m} \times 1.14\text{ m}$  grid.

**Data Collection:** The laptops connected to the six receiver antennas measure the Channel State Information (CSI) using CSI-Tool [26]. For all our experiments, we first measure the CSI magnitude on the RX grid in the absence of the edge lattice followed by measurements with the edge lattice placed in front of the TX. We then take the log-ratio of the latter to the former to compute the RSSI ratio, which is commonly utilized in the field programming literature to measure focusing efficiency [2].

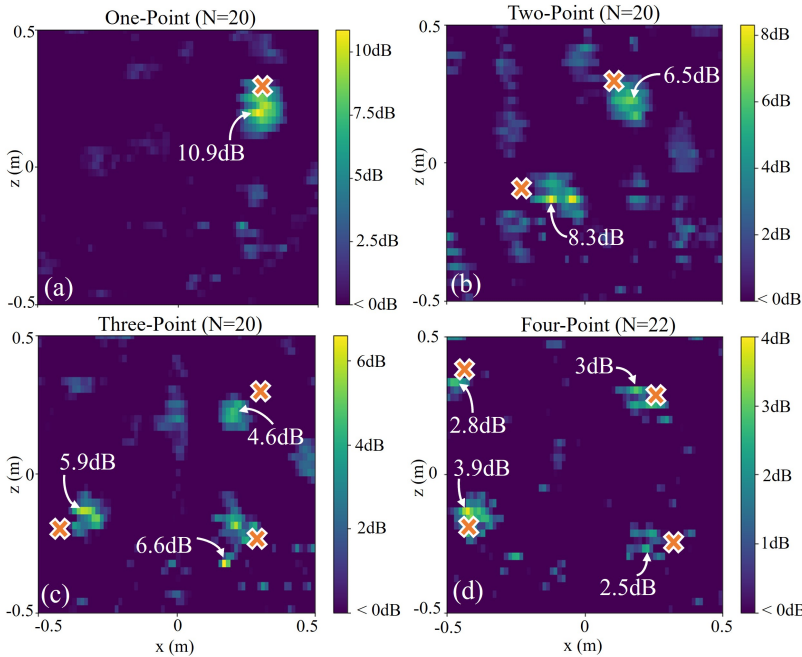
**Experimental Areas:** We conduct our experiments in three indoor environments (Fig. 9). Area 1 is an  $8\text{ m} \times 5\text{ m}$  conference room (also shown in Fig. 8), Area 2 is the lobby of a building of dimensions  $4.5\text{ m} \times 6\text{ m}$ , while Area 3 is a lab environment with dimensions  $3\text{ m} \times 4\text{ m}$ . All areas exhibit considerable multipath due to the proximity of large walls and furniture to the measurement apparatus. The fact that

our proposed approach produces strong focusing in these environments underscores its robustness and shows the low barrier-to-entry of our edge lattice in real life deployment. It is worth noting that our edge lattice design does not need any prior measurements in the operating environment.

### 5.3 Experimental Results

**Area 1 (Conference Room):** Fig. 10 shows the performance of our proposed paradigm for one-, two-, three-, and four-point focusing in Area 1 (see Fig. 9 for details). **All results of the paper are best viewed in color PDF.** The red “x” mark the desired focal points, while the white arrows point to the actual locations of the measured peaks of the RSSI ratio. The results demonstrate that our proposed approach can perform the desired multi-point focusing with a high quality. We note that the edge lattice is  $N=20$  for one-, two-, and three-point focusing, while it is  $N=22$  for four-point focusing. As we increase the number of desired focal points, the size of the lattice should increase in order to have enough control knobs to accomplish the given focusing task with a high-enough quality. We discuss the impact of the size of the lattice in more details later in this section. We do note that there is a small offset between the location of the measured peaks of the RSSI ratio and the desired target points. We largely ascribe this localization error to our synthesized measurement setup.

**Area 2 (Lobby):** To further demonstrate the robustness of our results, we run the two- and three-point focusing experiments in another environment, the lobby area of Fig. 9. Fig. 11 shows the corresponding results, confirming a strong focusing quality. Similarly, four-point focusing achieved 2.5 dB,

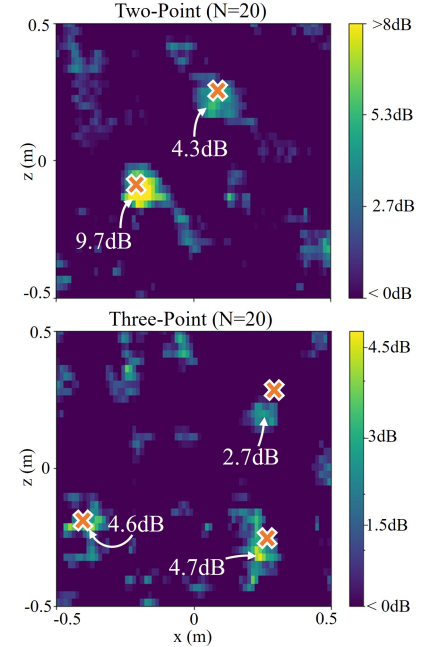


**Figure 10: Experimental results for one-, two-, three-, and four-point focusing of real-world experiments in Area 1 of Fig. 8 (conference room). See color PDF for proper viewing. Red “x” marks desired focal points, while white arrows point to the actual peak locations.**

3.9 dB, 4.9 dB, and 2.6 dB of gain at the focal points, which are comparable to the ones achieved in Area 1. It is interesting to note that two-point focusing produced better results in Area 2 as compared to Area 1, while three-point focusing was stronger in Area 1.

**Area 3 (Laboratory):** Finally, we tested the performance of the pipeline for three-point focusing in Area 3 of Fig. 9. Although this environment experiences more severe multipath due to more adjacent walls, the edge lattice achieved high focusing gains of 8.7 dB, 6.9 dB, and 4.9 dB near the desired focal points.

**Wide-Angle Focusing:** In the previous results, the desired focal points had a maximum deviation angle of  $26^\circ$  with respect to the center of the edge lattice. In some applications, we may be interested in wide-angle focusing, *i.e.*, focusing to the far sides. To demonstrate the ability to focus at wide angles, we next run experiments where the focal points are at wide angles w.r.t the center of the lattice, as shown in Fig. 9 (a). Fig 12 shows the results for wide angle focusing in Area 1 for one and two focal points, at the maximum angles of  $48^\circ$  and  $53^\circ$ , respectively. As can be seen, while it is more challenging to achieve wide-angle focusing, as expected, the results still show high-gain focusing even at the wide angles. It is worth noting that for these results, the RX grid was centered at  $x = -0.6$  and  $y = 1.9$ , and rotated by  $45^\circ$ . As

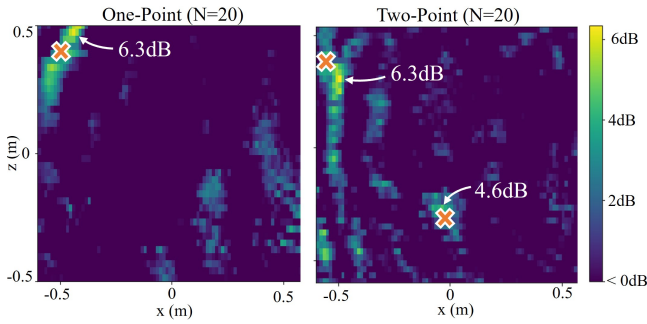


**Figure 11: Results for (top) two- and (bottom) three-point focusing in Area 2 (lobby). See color PDF for proper viewing.**

such, these results demonstrate focusing when the RX grid is not parallel to the edge matrix.

**Impact of Lattice Size:** We next show the impact of the size of the lattice on focusing quality. For this purpose, we consider the task of single-point focusing. We use the same setup as in Fig. 8 (Area 1), but we reduce the size of the lattice from  $N = 20$  to  $N = 12$ . Fig. 13 (left) shows the focusing result with  $N = 12$ , while the right figure reproduces the original  $N = 20$  result of single-point focusing of Fig. 10 (a), for comparison. While the focusing quality for  $N = 12$  is reasonable (gain of 6.4 dB), we can clearly see that the larger lattice produces a stronger, cleaner focusing (gain of 10.9 dB). This raises an interesting question on the minimum required lattice size to focus at  $K$  points. As the number of desired focal points increases, the minimum required lattice size to achieve a given performance quality shall increase. Furthermore, for a given  $K$ , the higher the required focusing gain, the larger the required lattice will become. Section 6 provides further discussion on the relationship between the lattice dimension  $N$  and its focusing capacity, leaving interesting explorations for future research.

**Impact of Additional Multipath:** So far, we showed experimental results in three areas of Fig. 9. These areas experience higher multipath than hallways/larger rooms, as confirmed in prior literature [42]. While we saw strong multi-point focusing in all these areas, the exact value of the



**Figure 12: Experimental results for wide angle focusing in Area 1 for (left) one and (right) two focal points. Note that the coordinate system is with respect to the tilted RX grid (see Fig. 9 (a)). See color PDF for proper viewing.**

focusing gains and the consequent focusing quality varied among the areas, as they experienced different amount of clutter. We next explicitly study the impact of clutter by running additional experiments in Area 1, while considerable furniture are placed near the experimental setup, as shown in Fig. 9 (b). Then, we employ the same edge lattice configurations used for generating Figs. 10 (b) and (c) and re-run the corresponding two- and three-point focusing experiments for comparison. Fig. 14 shows that while the overall focusing gains remain strong, the focusing is more noisy and with larger errors in the focusing locations as compared to Fig. 10 (b) and (c), as expected.

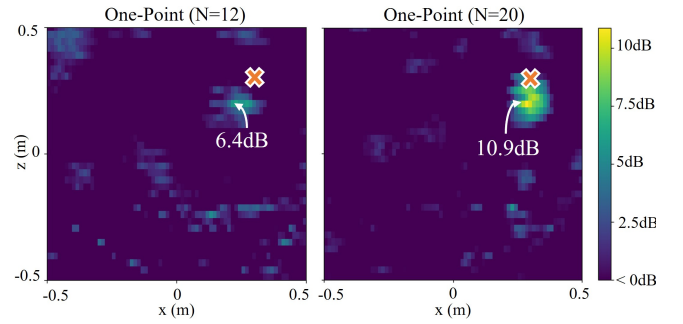
Overall, this section confirmed with 13 experiments that our methodology can achieve high-gain, multi-point focusing, showing its great potential for RF field programming.

## 6 DISCUSSION AND FUTURE WORK

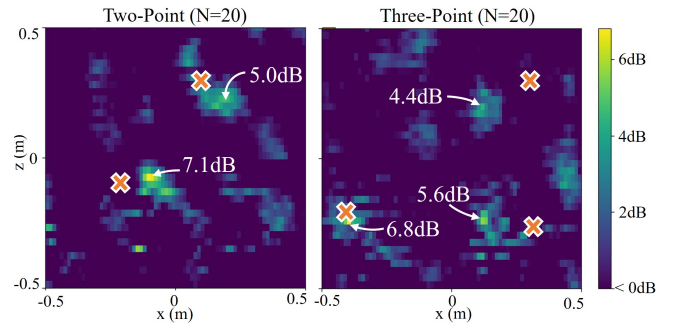
We next discuss several interesting aspects related to our proposed edge lattice concept, to motivate future work.

**Focal Capacity:** As demonstrated in Section 5.3, larger dimensions of the edge lattice ( $N$ ) can lead to stronger focusing. This then raises an interesting question: what is the minimum required lattice size to achieve focusing at a given number of points, and with a certain quality? As we increase the number of desired focal points, the size of the lattice should increase in order to have enough control knobs to accomplish the given focusing task with a high-enough quality. Characterization of the focal capacity of an edge lattice, *i.e.*, the achievable number of focal points with a given quality, is an interesting exploration and part of future work.

**Focal Error:** We report an average localization error of 8.4 cm with a standard deviation of 2.1 cm. Simulations of the lattice on Ansys HFSS showed much lesser errors (2.13 cm on average) suggesting that the manual construction of the edge lattice contributes to the error, in addition to the longer wavelength.



**Figure 13: Impact of lattice size – Focusing with a lattice of size (left)  $N = 12$  and (right)  $N = 20$ . See color PDF for proper viewing.**



**Figure 14: Impact of excessive clutter – (left) two- and (right) three-point focusing with additional clutter of Fig. 9 (b). Compare (left) to Fig. 10 (b) and (right) to Fig. 10 (c). See color PDF for proper viewing.**

**Edge Orientation Robustness:** HFSS simulations show that our method is robust to error in edge orientation up to  $10^\circ$ . Furthermore, despite chipping of the ABS frame due to heavy reuse of metal plates between experiments, we observed robust results as shown.

**Cost/Scalability Comparison:** The material for our edge lattice with 400 elements costs \$86.50 and was manufactured using ubiquitous machinery (shears and a 3D printer). In comparison, other works (*e.g.*, Table 1) require specialized, costly manufacturing pipelines, leveraging technologies such as UV photolithography, Electron Beam Evaporation (EBE) and/or nanofabrication [40, 64], and components for patch antenna based designs, a popular design paradigm, can also drive up cost. For example, [54] reports \$2/element after scaling, while our elements cost only \$0.25 each without scaling. While scaling these approaches can reduce costs, our approach can benefit more from scaling, as we require fewer, more common raw materials (steel/ABS vs. titanium/gold/LC-NJU-LDN-4), and less specialized manufacturing.

**Partitioning Algorithm Analysis:** In Section 4.2, we showed how to partition the edge elements to subsets such that each subset focuses on one of the given focal points (plus an idle subset). In doing so, we set forth the optimization problem of Eq. 5, which aimed at balancing the number of

edge elements allocated to each focal point (second term), while encouraging partitions that are spatially connected (first term). We then proposed Algorithm 2 to efficiently solve this problem (see Fig. 6 for sample convergence time).

In Fig. 6, we showed that our partitioning algorithm converged in just over a minute when executed on a 4th-Gen Intel i7 CPU. More generally, the algorithm's computational complexity is  $O(1)$  for single iteration. The number of iterations for convergence depends on the scheduling of the temperature parameter. Thus, the iteration number can be further reduced at the risk of missing global optimums.

Algorithm 2 aims to produce partitions which are both equally sized and spatially grouped. However, by adding weighting factors to the two terms of this objective, we can give more importance to either spatial connectivity or equal resource allocation. Furthermore, by suitably modifying the second term in Eq. 5, we can tune the extent of edge lattice resources allocated to a particular focal point. A study of the correlation between the choice of the objective function and diversity/quality of the generated fields would be an interesting future exploration.

We further note that Eq. 4 and the subsequent proposed focusing approach only needed to consider the phase of the radiated field on the Keller cone, making it immune to any modeling error in the diffracted signal magnitude, such as the variation of  $D$  in Eq. 3 with the incident angle. Developing other optimization objectives that also exploit the diffracted signal magnitude, as well as a corresponding sensitivity analysis can be an interesting future direction. Finally, we have set  $e_{ij} = [0, 0, 1]$  for those edges that need to be in an idle state, based on our initial empirical studies that showed this state to amplify focusing quality. A further characterization of this would be an interesting future direction.

**Complete Edge Element Modeling:** In this paper, we modeled the re-radiation pattern of our edge element as a single cone. In reality, the diffracted pattern will have some spread (*i.e.*, thickness) around the cone due to the finite edge length and the local nature of wave propagation [5]. Furthermore, the edge element may affect the electromagnetic field through modes other than diffraction off of the primary edge, such as diffraction off of the other edges and (possibly non-specular) reflection off of the plate's faces. Preliminary simulation-based studies indicate that the edge element's exact scattering pattern can be a function of the distance from the TX to the element, the orientation of the element, the aspect ratio of the element, and the exact element dimensions, among other factors. Developing a model which accounts for all these factors presents an interesting and challenging future direction. In solving our multi-focus optimization problem, a more comprehensive edge model (such as UTD [36]) would allow for the quantification of the impact of an edge element ( $i, j$ ) on targets other than  $a_{ij}$  (which is

currently ignored). Considering the specific material which constitutes the edge would also improve modeling accuracy.

**Reconfigurability with Advanced Materials:** In this paper, we laid out the foundation of a new concept, that a lattice of cheap off-the-shelf edge elements can provide a rich space for programming the RF field. Being the first paper on this topic, we opted to manually place the edges in the angled slots of the frame. The next step in this research would be to make this architecture reconfigurable. While there are many ways to accomplish this, such as utilizing traditional actuators that place each edge element in the right angle, utilizing smart materials that respond to an external stimulus can provide an efficient way of designing a reconfigurable edge lattice. This can be realized by an array of linear contraction actuators, such as Liquid Crystal Elastomers (LCEs), which reversibly contract upon application of heat and/or light, where the amount of contraction can be tuned proportional to the area exposed to the laser/stimulus [32]. Alternatively, a small-scale phased array antenna can be utilized as an active feed to steer a relatively wide initial beam, which is then shaped by a suitably optimized edge lattice for dynamic multi-focusing. Further exploration of this can thus be an exciting future direction. It is worth noting that all the existing work that showed focusing on 4 directions (see Fig. 1) implemented their design in a manual, non-reconfigurable manner.

## 7 CONCLUSIONS

In this paper, we presented a novel paradigm in the field of intelligent surfaces which employs the directivity of edge diffraction and the resulting Keller cones to create desired RF field patterns. More specifically, we showed that a lattice of edge elements can provide a rich set of "knobs" for RF field programming, via changing the orientation of the edge elements and exploiting the exiting Keller cones. We further proposed an efficient algorithm to configure the orientations of the edges and achieve multi-point focusing. We then built sample prototypes of our proposed design, using off-the-shelf material (*i.e.*, metal plates costing 7 cents) and extensively validated the proposed paradigm with 13 experiments in 3 different indoor environments. Our results showed how an edge lattice can focus the transmitted signal of a WiFi card of a laptop on up to and including 4 focal points, with a peak gain of 10.9 dB in the CSI magnitude. We further experimentally showed the impact of many different factors, such as size of the lattice, steering angle of the focal point, and environmental factors, on the performance. Overall, the paper showed the rich potential of edges for RF field programming.

## 8 ACKNOWLEDGEMENTS

We thank the anonymous reviewers and Shepherd for valuable comments and suggestions. This work is funded in part by ONR award N00014-20-1-2779 and in part by NSF NeTS award 1816931.

## REFERENCES

- [1] G. C. Alexandropoulos, N. Shlezinger, and P. Del Hougne. Reconfigurable intelligent surfaces for rich scattering wireless communications: Recent experiments, challenges, and opportunities. *IEEE Communications Magazine*, 59(6):28–34, 2021.
- [2] V. Arun and H. Balakrishnan. RFocus: Beamforming Using Thousands of Passive Antennas. In *NSDI*, pages 1047–1061, 2020.
- [3] L. Bao, R. Y. Wu, X. Fu, Q. Ma, G. D. Bai, J. Mu, R. Jiang, and T. J. Cui. Multi-beam forming and controls by metasurface with phase and amplitude modulations. *IEEE Transactions on Antennas and Propagation*, 67(10):6680–6685, 2019.
- [4] D. Berry, R. Malech, and W. Kennedy. The reflectarray antenna. *IEEE Transactions on Antennas and Propagation*, 11(6):645–651, 1963.
- [5] H. L. Bertoni. *Radio propagation for modern wireless systems*. Pearson Education, 1999.
- [6] E. Björnson, E. G. Larsson, and T. L. Marzetta. Massive MIMO: Ten myths and one critical question. *IEEE Communications Magazine*, 54(2):114–123, 2016.
- [7] E. Björnson, Ö. Özdogan, and E. G. Larsson. Intelligent reflecting surface versus decode-and-forward: How large surfaces are needed to beat relaying? *IEEE Wireless Communications Letters*, 9(2):244–248, 2019.
- [8] E. Björnson, L. Sanguinetti, H. Wymeersch, J. Hoydis, and T. L. Marzetta. Massive MIMO is a reality—What is next?: Five promising research directions for antenna arrays. *Digital Signal Processing*, 94:3–20, 2019.
- [9] E. Björnson, H. Wymeersch, B. Matthiesen, P. Popovski, L. Sanguinetti, and E. de Carvalho. Reconfigurable intelligent surfaces: A signal processing perspective with wireless applications. *IEEE Signal Processing Magazine*, 39(2):135–158, 2022.
- [10] J. Butler. Beam-forming matrix simplifies design of electronically scanned antennas. *Electronic design*, 9:170–173, 1961.
- [11] J. Chan, C. Zheng, and X. Zhou. 3D printing your wireless coverage. In *Proceedings of the 2nd International Workshop on Hot Topics in Wireless*, pages 1–5, 2015.
- [12] W. C. Chew. *Waves and fields in inhomogeneous media*, volume 16. John Wiley & Sons, 1999.
- [13] K. W. Cho, M. H. Mazaheri, J. Gummesson, O. Abari, and K. Jamieson. mmWall: A Transflective Metamaterial Surface for mmWave Networks. *arXiv preprint arXiv:2209.11554*, 2022.
- [14] F. H. Danufane, M. Di Renzo, J. De Rosny, and S. Tretyakov. On the path-loss of reconfigurable intelligent surfaces: An approach based on Green's theorem applied to vector fields. *IEEE Transactions on Communications*, 69(8):5573–5592, 2021.
- [15] S. Dathanasombat, A. Prata, L. Arnaro, J. Harrell, S. Spitz, and J. Perret. Layered lens antennas. In *IEEE Antennas and Propagation Society International Symposium. 2001 Digest. Held in conjunction with: USNC/URSI National Radio Science Meeting (Cat. No. 01CH37229)*, volume 2, pages 777–780. IEEE, 2001.
- [16] P. P. de la Torre, M. Sierra-Castaner, and M. Sierra-Perez. Design of a double array lens. In *2006 First European Conference on Antennas and Propagation*, pages 1–5. IEEE, 2006.
- [17] M. Di Renzo and A. I. Aravanis. *Catching the 6G Wave by Using Metamaterials*, chapter 6, pages 69–87. John Wiley & Sons, Ltd, 2021.
- [18] M. Di Renzo, F. H. Danufane, X. Xi, J. De Rosny, and S. Tretyakov. Analytical modeling of the path-loss for reconfigurable intelligent surfaces—anomalous mirror or scatterer? In *2020 IEEE 21st International Workshop on Signal Processing Advances in Wireless Communications (SPAWC)*, pages 1–5. IEEE, 2020.
- [19] M. Di Renzo, M. Debbah, D.-T. Phan-Huy, A. Zappone, M.-S. Alouini, C. Yuen, V. Sciancalepore, G. C. Alexandropoulos, J. Hoydis, H. Gacanin, et al. Smart radio environments empowered by reconfigurable AI metasurfaces: An idea whose time has come. *EURASIP Journal on Wireless Communications and Networking*, 2019(1):1–20, 2019.
- [20] M. Di Renzo, A. Zappone, M. Debbah, M.-S. Alouini, C. Yuen, J. De Rosny, and S. Tretyakov. Smart radio environments empowered by reconfigurable intelligent surfaces: How it works, state of research, and the road ahead. *IEEE Journal on Selected Areas in Communications*, 38(11):2450–2525, 2020.
- [21] M. Dunna, C. Zhang, D. Sievenpiper, and D. Bharadia. ScatterMIMO: Enabling virtual MIMO with smart surfaces. In *Proceedings of the 26th Annual International Conference on Mobile Computing and Networking*, pages 1–14, 2020.
- [22] C. Feng, X. Li, Y. Zhang, X. Wang, L. Chang, F. Wang, X. Zhang, and X. Chen. RFlens: metasurface-enabled beamforming for IoT communication and sensing. In *Proceedings of the 27th Annual International Conference on Mobile Computing and Networking*, pages 587–600, 2021.
- [23] R. L. Forward. Roundtrip interstellar travel using laser-pushed light-sails. *Journal of Spacecraft and Rockets*, 21(2):187–195, 1984.
- [24] S. Gong, X. Lu, D. T. Hoang, D. Niyato, L. Shu, D. I. Kim, and Y.-C. Liang. Toward smart wireless communications via intelligent reflecting surfaces: A contemporary survey. *IEEE Communications Surveys & Tutorials*, 22(4):2283–2314, 2020.
- [25] G. Gradoni, M. Di Renzo, A. Diaz-Rubio, S. Tretyakov, C. Caloz, Z. Peng, A. Alu, G. Lerosey, M. Fink, V. Galdi, et al. Smart radio environments. *arXiv preprint arXiv:2111.08676*, 2021.
- [26] D. Halperin, W. Hu, A. Sheth, and D. Wetherall. Tool release: gathering 802.11n traces with channel state information. *Comput. Commun. Rev.*, 41:53, 2011.
- [27] S. Hu, F. Rusek, and O. Edfors. Beyond Massive MIMO: The potential of data transmission with large intelligent surfaces. *IEEE Transactions on Signal Processing*, 66(10):2746–2758, 2018.
- [28] J. Huang. The finite ground plane effect on the microstrip antenna radiation patterns. *IEEE Transactions on Antennas and Propagation*, 31(4):649–653, 1983.
- [29] J. Huang and J. A. Encinar. *Reflectarray antennas*. John Wiley & Sons, 2007.
- [30] J. Huang and R. J. Pogorzelski. A Ka-band microstrip reflectarray with elements having variable rotation angles. *IEEE transactions on antennas and propagation*, 46(5):650–656, 1998.
- [31] I. Iliopoulos, M. Teniou, M. Casaletti, P. Potier, P. Pouliguen, R. Sauleau, and M. Ettore. Near-field multibeam generation by tensorial metasurfaces. *IEEE Transactions on Antennas and Propagation*, 67(9):6068–6075, 2019.
- [32] H. Jiang, C. Li, and X. Huang. Actuators based on liquid crystalline elastomer materials. *Nanoscale*, 5 12:5225–40, 2013.
- [33] A. Kelkar. FLAPS: conformal phased reflecting surfaces. In *Proceedings of the 1991 IEEE National Radar conference*, pages 58–62. IEEE, 1991.
- [34] J. B. Keller. Geometrical theory of diffraction. *Journal of the Optical Society of America*, 52(2):116–130, 1962.
- [35] W. Khawaja, O. Ozdemir, Y. Yapici, F. Erden, and I. Guvenc. Coverage enhancement for NLOS mmWave links using passive reflectors. *IEEE Open Journal of the communications Society*, 1:263–281, 2020.
- [36] R. G. Kouyoumjian and P. H. Pathak. A uniform geometrical theory of diffraction for an edge in a perfectly conducting surface. *Proceedings of the IEEE*, 62(11):1448–1461, 1974.
- [37] E. G. Larsson, O. Edfors, F. Tufvesson, and T. L. Marzetta. Massive MIMO for next generation wireless systems. *IEEE communications magazine*, 52(2):186–195, 2014.
- [38] Z. Li, Y. Xie, L. Shangguan, R. I. Zelaya, J. Gummesson, W. Hu, and K. Jamieson. Towards programming the radio environment with large arrays of inexpensive antennas. In *16th USENIX Symposium on Networked Systems Design and Implementation (NSDI 19)*, pages

- 285–300, 2019.
- [39] F. Liu, D.-H. Kwon, and S. A. Tretyakov. Reflectarrays and metasurface reflectors as diffraction gratings. *arXiv preprint arXiv:2202.09029*, 2022.
- [40] S. Liu, T. J. Cui, L. Zhang, Q. Xu, Q. Wang, X. Wan, J. Q. Gu, W. X. Tang, M. Qing Qi, J. G. Han, et al. Convolution operations on coding metasurface to reach flexible and continuous controls of terahertz beams. *Advanced Science*, 3(10):1600156, 2016.
- [41] Y. Liu, X. Mu, J. Xu, R. Schober, Y. Hao, H. V. Poor, and L. Hanzo. STAR: Simultaneous transmission and reflection for 360° coverage by intelligent surfaces. *IEEE Wireless Communications*, 28(6):102–109, 2021.
- [42] M. Malmirchegini and Y. Mostofi. On the Spatial Predictability of Communication Channels. *IEEE Transactions on Wireless Communications*, 11(3):964–978, March 2012.
- [43] T. L. Marzetta and H. Yang. *Fundamentals of Massive MIMO*. Cambridge University Press, 2016.
- [44] D. T. McGrath. A lightweight constrained lens for wide angle scan in two planes. In *Illinois Univ. Proceedings of the Antenna Applications Symposium held in Urbana, Illinois*, 1987.
- [45] Q.-U.-A. Nadeem, A. Kammoun, A. Chaaban, M. Debbah, and M.-S. Alouini. Intelligent reflecting surface assisted wireless communication: Modeling and channel estimation. *arXiv preprint arXiv:1906.02360*, 2019.
- [46] Nature. Metasurfaces go mainstream. <https://www.nature.com/articles/s41566-022-01137-1>, Dec 2022. [Online; accessed 7-March-2023].
- [47] NTT-DOCOMO. DOCOMO conducts world’s first successful trial of transparent dynamic metasurface. [https://www.docomo.ne.jp/english/info/media\\_center/pr/2020/0117\\_00.html](https://www.docomo.ne.jp/english/info/media_center/pr/2020/0117_00.html), 2020. [Online; accessed 26-February-2023].
- [48] Ö. Özdoğan, E. Björnson, and E. G. Larsson. Intelligent reflecting surfaces: Physics, propagation, and pathloss modeling. *IEEE Wireless Communications Letters*, 9(5):581–585, 2019.
- [49] A. Pallaprolu, B. Korany, and Y. Mostofi. Wiffract: a new foundation for RF imaging via edge tracing. In *Proceedings of the 28th Annual International Conference on Mobile Computing And Networking*, pages 255–267, 2022.
- [50] C. Pan, H. Ren, K. Wang, J. F. Kolb, M. Elkhachlan, M. Chen, M. Di Renzo, Y. Hao, J. Wang, A. L. Swindlehurst, et al. Reconfigurable Intelligent Surfaces for 6G Systems: Principles, Applications, and Research Directions. *IEEE Communications Magazine*, 59(6):14–20, 2021.
- [51] D. M. Pozar, S. D. Targonski, and H. Syrigos. Design of millimeter wave microstrip reflectarrays. *IEEE transactions on antennas and propagation*, 45(2):287–296, 1997.
- [52] K. Qian, L. Yao, X. Zhang, and T. N. Ng. MilliMirror: 3D printed reflecting surface for millimeter-wave coverage expansion. In *Proceedings of the 28th Annual International Conference on Mobile Computing And Networking*, pages 15–28, 2022.
- [53] Y. Rahmat-Samfi. Keller’s cone encountered at a hotel. *IEEE Antennas and Propagation Magazine*, 49(6):88–89, 2007.
- [54] M. Rossanese, P. Mursia, A. Garcia-Saavedra, V. Sciancalepore, A. Asadi, and X. Costa-Perez. Designing, building, and characterizing RF switch-based reconfigurable intelligent surfaces. In *Proceedings of the 16th ACM Workshop on Wireless Network Testbeds, Experimental evaluation & CHaracterization*, pages 69–76, 2022.
- [55] W. Saad, M. Bennis, and M. Chen. A Vision of 6G Wireless Systems: Applications, Trends, Technologies, and Open Research Problems. *IEEE Network*, 34(3):134–142, 2020.
- [56] T. Senior and P. Uslenghi. Experimental detection of the edge-diffraction cone. *Proceedings of the IEEE*, 60(11):1448–1448, 1972.
- [57] C. Shepard, H. Yu, N. Anand, E. Li, T. Marzetta, R. Yang, and L. Zhong. Argos: Practical many-antenna base stations. In *Proceedings of the 18th Annual International Conference on Mobile Computing and Networking*, pages 53–64, 2012.
- [58] T. Tatarenko. Proving convergence of log-linear learning in potential games. In *2014 American Control Conference*, pages 972–977, 2014.
- [59] N. M. Tran, M. M. Amri, J. H. Park, G. R. Faqih, D. I. Kim, and K. W. Choi. Beam Splitting Technique for Reconfigurable Intelligent Surface-Aided Simultaneous Wireless Information and Power Transfer Applications. In *2022 IEEE Information Theory Workshop (ITW)*, pages 61–65. IEEE, 2022.
- [60] N. M. Tran, M. M. Amri, J. H. Park, D. I. Kim, and K. W. Choi. Multifocus Techniques for Reconfigurable Intelligent Surface-Aided Wireless Power Transfer: Theory to Experiment. *IEEE Internet of Things Journal*, 9(18):17157–17171, 2022.
- [61] H. L. Van Trees. *Optimum array processing: Part IV of detection, estimation, and modulation theory*. John Wiley & Sons, 2002.
- [62] H. Wang, Y. Li, H. Chen, Y. Han, S. Sui, Y. Fan, Z. Yang, J. Wang, J. Zhang, S. Qu, et al. Multi-beam metasurface antenna by combining phase gradients and coding sequences. *IEEE Access*, 7:62087–62094, 2019.
- [63] A. Welkie, L. Shangquan, J. Gummeson, W. Hu, and K. Jamieson. Programmable radio environments for smart spaces. In *Proceedings of the 16th ACM Workshop on Hot Topics in Networks*, pages 36–42, 2017.
- [64] J. Wu, Z. Shen, S. Ge, B. Chen, Z. Shen, T. Wang, C. Zhang, W. Hu, K. Fan, W. Padilla, et al. Liquid crystal programmable metasurface for terahertz beam steering. *Applied physics letters*, 116(13):131104, 2020.
- [65] Q. Wu, S. Zhang, B. Zheng, C. You, and R. Zhang. Intelligent reflecting surface-aided wireless communications: A tutorial. *IEEE Transactions on Communications*, 69(5):3313–3351, 2021.
- [66] X. Wu, F. Hou, Y. Li, S. Zhao, S. Zhang, H. Xue, M. Chang, J. Han, H. Liu, and L. Li. Multitarget Wireless Power Transfer System Strategy Based on Metasurface-Holography Multifocal Beams. *IEEE Transactions on Microwave Theory and Techniques*, 2023.
- [67] X. Xiong, J. Chan, E. Yu, N. Kumari, A. A. Sani, C. Zheng, and X. Zhou. Customizing indoor wireless coverage via 3D-fabricated reflectors. In *Proceedings of the 4th ACM International Conference on Systems for Energy-Efficient Built Environments*, pages 1–10, 2017.
- [68] H.-X. Xu, T. Cai, Y.-Q. Zhuang, Q. Peng, G.-M. Wang, and J.-G. Liang. Dual-mode transmissive metasurface and its applications in multi-beam transmitarray. *IEEE Transactions on Antennas and Propagation*, 65(4):1797–1806, 2017.
- [69] X. Yang, S. Xu, F. Yang, M. Li, H. Fang, Y. Hou, S. Jiang, and L. Liu. A mechanically reconfigurable reflectarray with slotted patches of tunable height. *IEEE Antennas and Wireless Propagation Letters*, 17(4):555–558, 2018.
- [70] A. Zappone, M. Di Renzo, X. Xi, and M. Debbah. On the optimal number of reflecting elements for reconfigurable intelligent surfaces. *IEEE Wireless Communications Letters*, 10(3):464–468, 2020.
- [71] H. Zhang and B. Di. Intelligent omni-surfaces: Simultaneous refraction and reflection for full-dimensional wireless communications. *IEEE Communications Surveys & Tutorials*, 2022.